UDC 536.722:621.762

Delong Xie*, Leyin Xiao, Feng Lin, Xiaoyi Pan, Yu Su, Xiaohu Fang, Haiqing Qin, Chao Chen
Guangxi Key Laboratory of Superhard Materials, Chinese National Engineering Research Center for Special Mineral Materials, China Nonferrous Metal Geology and Mining Co, Ltd, Guilin, China
**xiedelonghn@foxmail.com*

Thermal analysis of FeCoCu pre-alloyed powders used for diamond tools

By simulating the pressureless sintering process, the thermal effects of FeCoCu pre-alloyed powders have been investigated. According to the notions of the Kissinger method, the activation energies in the expansion-shrinkage conversion stage are analyzed. Results show that with Fe content increasing, the specimens' specific heat capacity values present the increasing trend. The 25 %Fe–15 %Co–60 %Cu specimens have negative enthalpy value at 10 and 20 °C/min heating rate but positive values at 30 °C/min. For the specimens with lower Cu content, the enthalpies are always positive. It is established that both the specific heat capacity and enthalpy are larger when at higher heating rates. The activation energy of the 65 %Fe–15 %Co–20 %Cu specimens is 10 times higher than that of the 25 %Fe–15 %Co–60 %Cu specimens and the 45 %Fe–15 %Co–40 %Cu specimens.

***Keywords**: pre-alloyed powder, specific heat capacity, enthalpy, activation energy.*

INTRODUCTION

Diamond tools are widely used in geological drilling, stone processing, semiconductor materials cutting, and ceramics grinding [1–3]. Diamond is fine particles, so the tools should be made by using binder materials through the sintering process. Nowadays, as the metal bonding matrix, FeCoCu pre-alloyed powders are major materials used in the manufacture of diamond tools [4, 5]. The basic advantage of FeCoCu pre-alloyed powders is the component uniformity because each alloying particle contains all the composition, so the segregation is basically avoided, therefore, the properties of diamond tools can be improved significantly. In addition, alloying can decrease the activation energy in the atomic diffusion process [6, 7], which reduces the sintering temperature and sintering time.

At present various sintering technologies and methods are used for diamond tools and the sintering process with a constant heating rate is a research hotspot [8]. Shi [9] considered that the relative density of the samples will be 80 % when the densification rate reaches the maximum and it agrees to the experimental results. Da Li et al. [10] studied the Master Sintering Curve (MSC) of rutile TiO_2 using constant heating rate dilatometry data based on the combined-stages sintering model; the results show that the MSC theory can be applied to predict the final density and to design a reproducible process to fabricate ceramics with required density. In the pressureless sintering process the samples shrinkage gradually and

the relative densities become larger with temperature increasing, then the samples' microstructures and mechanical properties have large changes. Those changes are relative to the thermal behaviors in the sintering process, and by analyzing the kinetic data, the sintering characters could be predicted [11]. In addition, under the hypothesizes such as equilibrium system, simple particle arrangement and circular cavity et al., the sintering models can be proposed [12]. In thermal analysis Differential Scanning Calorimetry (DSC) is used widely [13–15]. The thermal parameters such as enthalpy, specific heat capacity and sintering activation energy et al. can be quantitative analysis based on DSC method.

To the best of our knowledge, little study has been reported on the thermal analysis of FeCoCu pre-alloyed powders in pressureless sintering process. This work reports the kinetic curves of three popular powders at a constant heating rate by means of DSC, analyzes the effect of Fe–Cu ratio on the kinetic behaviors, as well as calculates the specific heat capacity and enthalpy by thermodynamics formulas. With the help of Kissinger method the activation energy has been derived.

EXPERIMENT

Pre-alloyed powders with three Fe–Cu ratios were prepared as the sintering samples. The powders were manufactured by the co-precipitation method and the powder's compositions are listed in Table 1. Every element were weighted by mass ratio and dissolved into deionized water to form $FeCl_2 \cdot 4H_2O$, $CoCl_2 \cdot 6H_2O$, and $CuCl_2 \cdot 2H_2O$. The concentration of the solution was 1.0 mol/L. Subsequently, the as-prepared solution was mixed with 1.0 mol/L oxalic acid solution (1:1 ratio) and added into the reaction vessel at the same flow rate. In this reaction, the synthesis temperature is controlled to be 50°C, with a pH of 2.0 adjusted by adding ammonia, and a reaction time of 20 min. After precipitating for 2 h, the FeCoCu compound oxalate precipitate was obtained. After filtering, washing, calcining and reducing, the pre-alloyed powders were formed. The surface morphology was examined using a JSM-6700F scanning electron microscope (SEM).

Firstly, the samples were made by cold isostatic pressing on these powders up to 250 MPa. Their green densities are about 70 % of their theoretical density. Then the B samples were grinded to particles in the mortar. After sieving, the particles with meshes 10 to 20 were chosen for the experiments. The sintering characters of three kinds of specimens were measured with the thermal analysis instrument (NETZSCH Co, Ltd, STA449C, German). Specimens were heated to 950 °C at the heating rate of 10, 20 and 30 °C/min in argon atmosphere, respectively. The argon flow rate is 45 mL/min.

Table 1. Mass ratio of the pre-alloyed powders

Powder	Fe, wt %	Cu, wt %	Co, wt %
A	25	60	15
B	45	40	15
C	65	20	15

RESULTS AND DISCUSSION

Powders' microstructure

The surface shapes of A, B, and C powders are shown in Fig. 1. It is found that all the shapes of three powders are irregular. The particles connect mutually and

form into various loose surfaces. In addition, it can be found that the powder A has the largest particle (Its Fisher particle size is in a range of 9.2 μm, compared with the powder B of 8.7 μm and the powder C of 5.2 μm, respectively). This is because of the reduction process to manufacture the powders. The powder with higher Cu concentration has lower recrystallization temperature, leading to faster processes for recrystallization and grain growth at the same reduction temperature, so the particle size is larger. Changes in particle size will affect the sintering characters.

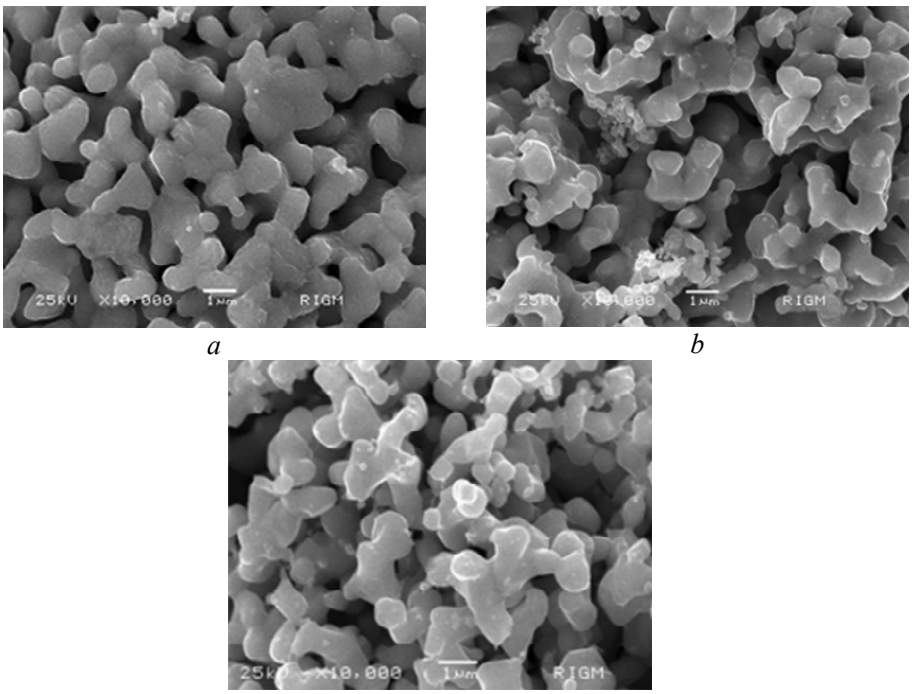

a *b*

c

Fig. 1. SEM pictures of the pre-alloyed powders: A (*a*), B (*b*), C (*c*).

DSC curves of three specimens at different heating rates

The DSC curves of the three kinds of specimens at different heating rates are shown in Fig. 2. It is found that all the three powders have endothermic process firstly, and then turn into exothermic process with temperature. The reason is that metal materials have a high thermal expansion coefficient, which is $11.7 \cdot 10^{-6}$ °C^{-1} for Fe, $12.5 \cdot 10^{-6}$ °C^{-1} for Co, and $16.6 \cdot 10^{-6}$ °C^{-1} for Cu, respectively. That's to say, the samples will expand when heated at the beginning, so the exothermic process occurs. When heated to a transition temperature the densification has happened, so the heat release begins. For the same specimens the peak value is higher and sharper at a higher heating rate, which is associated with that, a larger heating power must be provided to guarantee the higher heating rate, so under the higher heating rate the heat flow is larger. Figure 2 also shows that with Fe content increasing, the heat flow is larger; especially the peak values of C specimens are obviously sharp. That is because the particle size of the powders is related to the thermal resistance. The specimens with coarse particle size have larger resistance [16], at the same heating condition the tested heat flows become lower. As shown in Fig. 1, the C powder has the finest particle size, then the thermal resistance of the C specimens is the lowest, so the heat flow is obvious in the DSC curves.

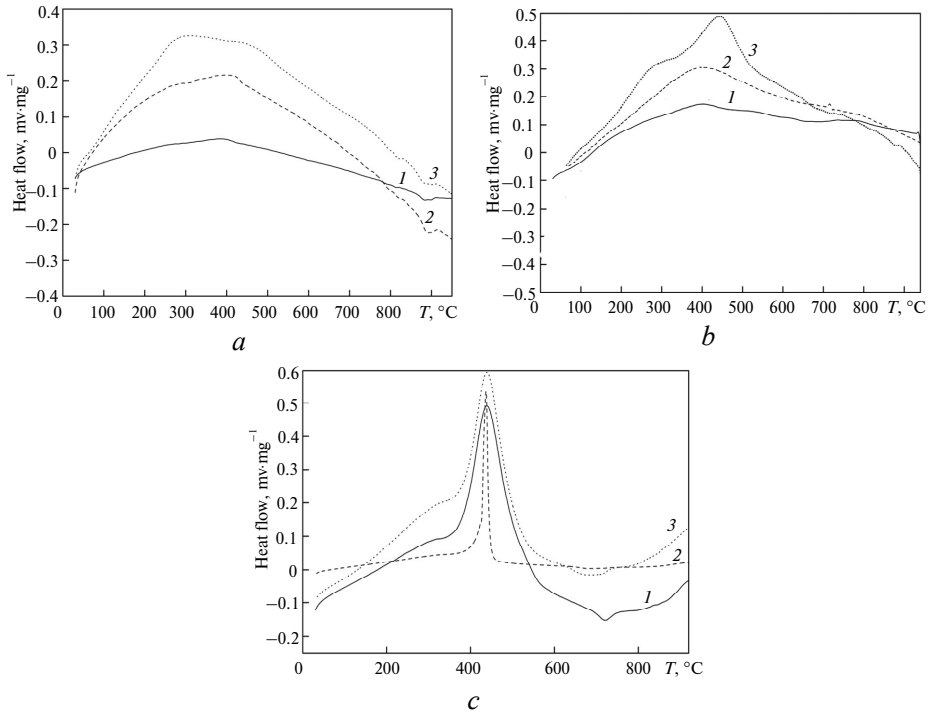

Fig. 2. DSC curves of three specimens (A (*a*), B (*b*), C (*c*)) at different heating rates: 10 (*1*), 20 (*2*), 30 (*3*) °C/min.

Specific heat capacity analysis

Heat capacity is an important parameter in thermodynamics and it can reflect the materials' physical properties. In the DSC experiments the gas flow of the argon is a certain value, so the constant pressure conditions could be considered. Based on the thermodynamics principle, when the materials have no physical changes, chemical reactions and non-volume work, the heat capacity is defined as follows:

$$c_p = \left(\frac{dH}{dT}\right)_p . \tag{1}$$

Specific heat capacity will be

$$c_p = \left(\frac{dH}{dT}\right)_p \cdot \frac{1}{m} . \tag{2}$$

By the mathematical derivation, the $\frac{dH}{dT}$ can be expressed as

$$\frac{dH}{dT} = \frac{dH}{dt} \Big/ \frac{dT}{dt} . \tag{3}$$

Then consider (5) into the expression (4), it will be

$$c_p = \left(\frac{dH}{dt} \Big/ \frac{dT}{dt}\right)_p \cdot \frac{1}{m}, \tag{4}$$

where H is the heat, T is the temperature, t is the time, and m is the weight.

According to the DSC testing principle, the ordinate of the DSC curves stands for the endothermic or exothermic heat in a unit time, that is to say, the ordinate means the enthalpy changes in unit time, which could be described $\frac{dH}{dt}$ in expression (2). In addition, the $\frac{dT}{dt}$ is the heating rate and m is the sample mass, then the c_p can be calculated by expression (4).

Figure 3 shows the specific heat capacity curves of the three specimens at different heating rates. It can be seen that the changes of the c_p curves are similar to the DSC curves. The c_p of all the three specimens increases with temperature, then begin to decrease when heated to a transition temperature. That is because in the pressureless sintering process, the specimens have the expansion and shrinkage stages. With Fe content increasing, the c_p values show the increasing trend, which is due to the thermal resistance as is mentioned above. The C specimens have the finest particle size so the thermal resistance is the lowest, then at the same heating condition the C particles have the largest heat flow in unit time, thus the c_p calculated is the highest. For the same specimens higher heating rates are related to the larger c_p. That is due to the reason that higher heating rate means the larger heating power, so the higher the heating rate is, the larger the c_p is.

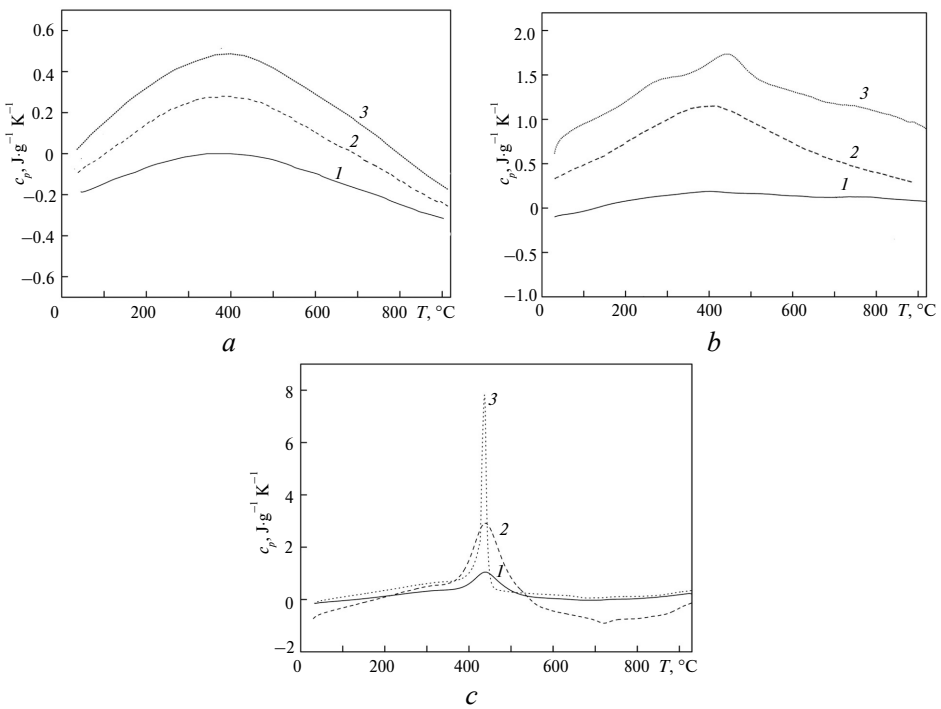

Fig. 3. The c_p curves of three specimens (A (*a*), B (*b*), C (*c*)) at different heating rates: 10 (*1*), 20 (*2*), 30 (*3*) °C/min.

Enthalpy analysis

The endothermic or exothermic heat in a certain temperature range can be calculated according to the formula below:

$$\Delta Q = \int_{t_1}^{t_2} \Delta P dt \,. \tag{5}$$

Because the ordinate means the enthalpy changes in unit time, so the enthalpy can be obtained by integrating the DSC curves:

$$\Delta H = \int_{t_1}^{t_2} \frac{dH}{dt} dt \,. \tag{6}$$

Figure 4 shows the enthalpy curves of the three specimens at different heating rates and Table 2 lists the specific enthalpy data. It can be seen that the higher heating rates correspond to the larger enthalpy. The enthalpy of *A* specimens at 10 °C/min is –132.61 KJ/mol, at 20 °C/min is –48.75 KJ/mol and at 30 °C/min it is –127.17 KJ/mol, respectively. The enthalpy of *B* specimens at 10 °C/min is 11.12 KJ/mol, at 20 °C/min is 149.96 KJ/mol and at 30 °C/min it is 164.17 KJ/mol, respectively. The enthalpy of C specimens at 10 °C/min is 57.49 KJ/mol, at 20 °C/min is 322.84 KJ/mol and at 30 °C/min is 456.18 KJ/mol, respectively. For the same specimens higher heating rates mean that the larger heating power, so the heat flows at higher heating rates are larger too, thus the enthalpies obtained are higher. For the *A* specimens when at the heating rates of 10 unit time 10 °C/min and 20 °C/min the enthalpy data are negative, but at 30 °C/min it is positive. The reason is that in the heating process the specimens have expansion and shrinkage stages, so there are endothermic and exothermic thermal effects. When heated at 10 and 20 °C/min, the endothermic effects are greater than the exothermic effects, so the enthalpies are negative values. But at 30 °C/min the sintering residence times in a certain temperature range are shorter, thus both the endothermic and exothermic thermal effects will carry out less sufficiently. Meanwhile the increasing heating power promotes the exothermic effects, so the endothermic effects are less than the exothermic effects. Therefore, the enthalpy is positive value. For B and C specimens the shrinkage degree increases and the expansion ratio decreases [17], leading to the exothermic effects larger than the endothermic effects, so the enthalpies of the two specimens are always the positive value. Under the same heating rates, the enthalpy of C specimens is larger than that of B and C specimens. That is because the C specimens have the lowest expansion ratio and the highest shrinkage degree, so the whole endothermic effects are obvious.

Table 2. The calculated enthalpies of three specimens at three heating rates

	Specimen								
	A			B			C		
Heating rate, °C/min	10	20	30	10	20	30	10	20	30
Enthalpy, KJ/mol	–132.61	–48.75	127.17	11.12	149.96	164.17	57.49	322.84	456.18

Activation energy analysis

Kissinger method is widely used in the thermal analysis [18]. According to the Kissinger theory, the relationships between the heating rates and the peaks of the DSC curves can be described as follows:

$$\frac{d[\log(\theta / Tp^2)]}{d(1/Tp)} = -\frac{E}{R}, \tag{7}$$

where θ is the heating rate, *Tp* is the curve peak, *E* is the activation energy, *R* is the constant, respectively.

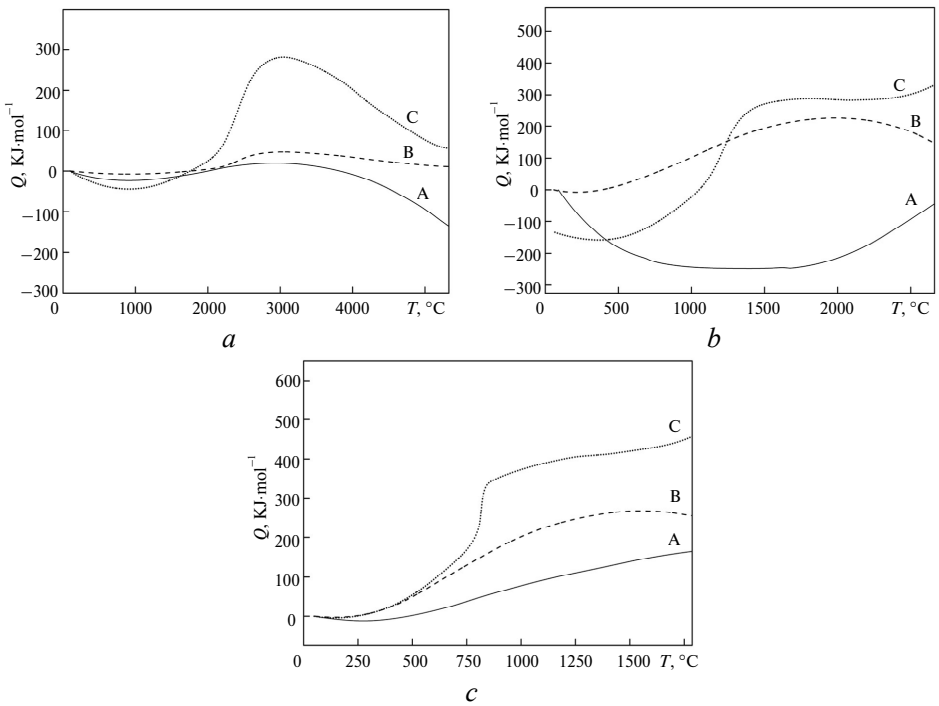

Fig. 4. Enthalpy curves of three specimens (A (*a*), B (*b*), C (*c*)) at different heating rates: 10 (*a*), 20 (*b*), 30 (*c*) °C/min.

At different heating rates, three will be:

$$\log\left(\frac{\theta_1}{Tp_1^2}\right)+\frac{E}{RTp_1}=\log\left(\frac{\theta_2}{Tp_2^2}\right)+\frac{E}{RTp_2}=\ldots, \tag{8}$$

θ_1, θ_2 are different heating rates, respectively.

Then draw the relationship chart between $\ln\left(\frac{\theta}{Tp^2}\right)$ and $1/Tp$, the activation energy in the expansion–shrinkage conversion stage can be obtained from the straight slope.

Table 3 shows the sintering kinetic data of the DSC curves. By drawing the relationship between $\ln\left(\frac{\theta}{Tp^2}\right)$ and $1/Tp$ in Table 3, Fig. 5 can be obtained. The activation energy of A specimens is 57.9 KJ/mol, B is 66.1 KJ/mol and C is 753.9 KJ/mol, respectively.

The results show that the activation energy of A specimen is close to B specimen, but that of C specimen is 10 times higher than A and B. The reason is that sintering process has relations with the materials' melting point. In powder metallurgical theory, the sintering temperature should be 60 to 70 % of the melting point. The melting point of Cu element is 1084 °C, compared with Fe is 1535 °C and Co is 1495 °C, respectively. In the C specimens Fe and Co are the bulk phases, thus, in the sintering process more energy must be provided.

Table 3. The sintering kinetic data at different heating rates by Kissinger method

Specimen	Heating rate , °C/min	*Tp*, °C	*Tp*, K	$(1/Tp)\cdot 10^3$, K^{-1}	$\ln\left(\frac{\theta}{Tp^2}\right)$
A	10	370	643.15	1.554847	–10.6302
	20	400	673.15	1.485553	–10.0282
	30	430	580.15	1.723692	–9.32538
B	10	392	665.15	1.50342	–10.6974
	20	406	679.15	1.472429	–10.046
	30	443	716.15	1.396356	–9.74658
C	10	436	709.15	1.410139	–10.8255
	20	440	713.15	1.40223	–10.1437
	30	442	715.15	1.398308	–9.74379

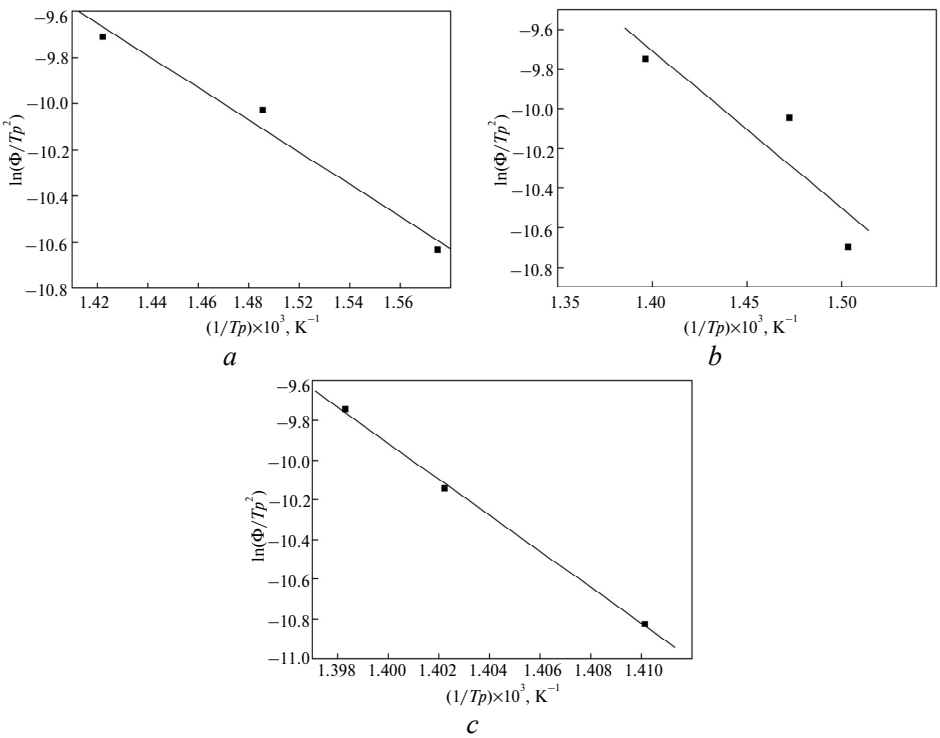

Fig. 5. Activation energy of the three specimens: A (*a*), B (*b*), C (*c*).

CONCLUSIONS

All the three kinds of powders have endothermic process firstly, then turn into exothermic process with temperature. With Fe content increasing, the heat flow is larger. For the same specimens the DSC curves are sharper when heated at higher heating rate.

The specific heat capacity curves of the three samples are similar to the DSC curves.

For the same specimens the higher heating rates correspond to the larger enthalpy. Due to the endothermic and exothermic thermal effects the highest Cu

content samples have the negative enthalpies at 10 and 20 °C/min, but have positive enthalpies at 30 °C/min.

The results show that activation energy of the 25 %Fe–15 %Co–60 %Cu specimens is close to the 45 %Fe–15 %Co–40 %Cu specimens, but that of the 65 %Fe–15 %Co–20 %Cu specimens is 10 times higher than the first two specimens.

ACKNOWLEDGMENTS

This work is supported by the Plan program of Scientific Research and Technical Development of Guilin in China (20150105-1).

При моделюванні процесу спікання без тиску досліджено термічні ефекти в попередньо легованих порошках FeCoCu. З використанням методу Кіссінджера проаналізовано енергію активації на стадії розширення–усадка. Результати показують, що при збільшенні вмісту Fe значення питомої теплоємності демонструють тенденцію до зростання. Зразки 25 %Fe–15 %Co–60 %Cu мають негативні значення ентальпії при швидкості нагріву 10 ° і 20 °С/хв, але позитивні при 30 °С/хв. Для зразків з меншим вмістом Cu ентальпія завжди позитивна. Встановлено, що питома теплоємність і ентальпія більші при більш високіх швидкостях нагрівання. Енергія активації зразків 65 %Fe–15 %Co–20 %Cu у 10 разів вища, ніж зразків 25 %Fe–15 %Co–60 %Cu і 45 %Fe–15 %Co–40 %Cu.

***Ключові слова**: попередньо легований порошок, питома теплоємність, ентальпія, енергія активації.*

При моделировании процесса спекания без приложения давления исследованы термические эффекты в предварительно легированных порошках FeCoCu. С использованием метода Киссинджера проанализирована энергия активации на стадии расширение–усадка. Результаты показывают, что с увеличением содержания железа значения удельной теплоемкости образцов демонстрируют тенденцию к повышению. Образцы 25 %Fe–15 %Co–60 %Cu имеют отрицательные значения энтальпии при скорости нагрева 10 и 20 °С/мин, но положительные при 30 °С/мин. Для образцов с меньшим содержанием Cu энтальпия всегда положительна. Установлено, что удельная теплоемкость и энтальпия больше при более высоких скоростях нагрева. Энергия активации образцов 65 %Fe–15 %Co–20 %Cu в 10 раз выше, чем образцов 25 %Fe–15 %Co–60 %Cu и 45 %Fe–15 %Co–40 %Cu.

***Ключевые слова**: предварительно легированный порошок, удельная теплоемкость, энтальпия, энергия активации.*

1. *Lavrinenko V. I., Sytnyk B. V., Poltoratskyi V. G., Bochechka O. O., Solod V. Yu.* Composites based on cBN micron powders structured by carbon binder for the application as functional elements in the working layer of diamond-abrasive tools. Part 2. Composites as bearing elements // J. Superhard Mater. – 2014. – **36**, N 5. – P. 338–343.
2. *Mechnyk V. A.* Diamond–Fe–Cu–Ni–Sn composite materials with predictable stable characteristics // Mater. Sci. – 2013. – **48**, N 5. – P. 591–600.
3. *Zaitsev A. A., Sidorenko D. A., Levashov E. A., Kurbatkina V. V., Andreev V. A., Rupasov S. I., and Sevast'yanov P. V.* Diamond tools in metal bonds dispersion-strengthened with nanosized particles for cutting highly reinforced concrete // J. Superhard Mater. – 2010. – **32**, N 6. – P. 423–431.
4. *Mechnik V. A.* Production of diamond−(Fe−Cu−Ni−Sn) composites with high wear resistance // Powder Metall. Met. Cer. – 2014. – **52**, N 9. – P. 577–587.
5. *Mechnyk V. A.* Regularities of structure formation in diamond−Fe–Cu–Ni–Sn–CrB_2 systems // Mater. Sci. – 2013. – **49**, N 1. – P. 93–101.
6. *Mechnik V. A.* Effect of hot recompaction parameters on the structure and properties of diamond–(Fe–Cu–Ni–Sn–CrB_2) composites // Powder Metall. Met. Cer
. – 2014. – **52**, N 11. – P. 709–721.
7. *Han P., Xiao F.-R, Zou W.-J., Liao B.* Influence of hot pressing temperature on the microstructure and mechanical properties of 75 %Cu–25 %Sn alloy // Mater. Des. – 2014. – **53**. – P. 38–42.

8. *Tomelini M.* Functional form of the Kolmogorov–Johnson–Mehl–Avrami kinetics for non-isothermal phase transformations at constant heating rate // Thermochim Act. – 2013. – **566**. – P. 249–256.
9. *Shi J. L.* Solid state sintering of ceramics: pore microstructure models, densification equations and applications // J. Mater. Sci. – 1999. – **34**. – P. 3801–3802.
10. *Li D., Chen S. O., Shao W. Q., Ge X., Zhang Y., Zhang Sh.* Densification evolution of TiO_2 ceramics during sintering based on the master sintering curve theory // Mater. Lett. – 2008. – **62**. – P. 849–851.
11. *Huang S. G., Li L., Vleugels J., Wang P., Van der Biest O.* Thermodynamic prediction of the nonstoichiometric phase ZrO_2–$CeO_{1.5}$–CeO_2 system // J. Eur. Ceram. Soc. – 2003. – **23**. – P. 99–106.
12. *Yüksei S., Kezban A., Müserref O.* A model for initial-stage sintering thermodynamics of an alumina powder // Powder Technol. – 2008. – **188**. – P. 9–12.
13. *Emily M. H., Michelle L. P.* Ignition dynamics and activation energies of metallic thermites: From nano- to micron–scale particulate composites // J. Appl. Phys. – 2005. – **98**. – P. 1–8.
14. *Fan R.-H., Liu B., Zhang J.-D., Bi J.-Q., Yin Y.-Sh.* Kinetic evaluation of combustion synthesis $3TiO_2 + 7Al \rightarrow 3TiAl + 2A1_2O_3$ using non–isothermal DSC method // Mater. Chem. Phys. – 2005. – **91**. – P. 140–145.
15. *Sanders J. P., Gallagher P. K.* Kinetic analysis using simultaneous TG/DSC measurements. Part II: Decomposition of calcium carbonate having different particle sizes // J. Therm. Anal. Calorim. – 2005. – **82**. – P. 659–664.
16. *Riko O., Hiroshi O., Moyuru O., Sadao T.* Thermal analysis of powdered alumina materials // Ibid. – 1997. – **49**. – P. 961–970.
17. *Xie D., Wan L., Song D., Wang Sh., Lin F., Pan X., Xu J.* Pressureless sintering curve and sintering activation energy of Fe–Co–Cu pre-alloyed powders // Mater. Des. – 2015. – **87**. – P. 482–487.
18. *Holubova J., Cernosek Z., Cernoskova E.* Crystallization of supercooled liquid of selenium: The comparison of kinetic analysis of both isothermal and non-isothermal DSC data // Mater. Lett. – 2006. – **60**. – P. 2429–2432.

Received 13.02.17